Observation of Inverted Phases in Poly(styrene-*b*-butadiene-*b*-styrene) Triblock Copolymer by Solvent-Induced Order−Disorder Phase Transition

Qingling Zhang,[†] Ophelia K. C. Tsui,*[,‡] Binyang Du,[†] Fajun Zhang,[†] Tao Tang,[†] and Tianbai He*[,†]

State Key Laboratory of Polymer Physics and Chemistry, Changchun Institute of Applied Chemistry, Chinese Academy of Sciences, Changchun, 130022, P. R. China, and Physics Department, Hong Kong University of Science and Technology, Clear Water Bay, Hong Kong, P. R. China

Received July 6, 2000; Revised Manuscript Received October 17, 2000

ABSTRACT: We report observation of inverted phases consisting of spheres and/or cylinders of the majority fraction block in a poly(styrene-*b*-butadiene-*b*-styrene) (SBS) triblock copolymer by solvent-induced order−disorder phase transition (ODT). The SBS sample has a molecular weight of 140K Da and a polystyrene (PS) weight fraction of 30%. Tapping mode atomic force microscopy (AFM) and transmission electron microscopy (TEM) were utilized to study the copolymer microstructure of a set of solution-cast SBS films dried with different solvent evaporation rates, *R*. The control with different *R* leads to kinetic frozen-in of microstructures corresponding to a different combination parameter $\chi_{eff}Z$ of the drying films (where χ_{eff} is the effective interaction parameter of the polymer solution in the cast film and *Z* the number of "blobs" of size equal to the correlation length one block copolymer chain contains), for which faster evaporation rates result in microstructures of smaller $\chi_{eff}Z$. As *R* was decreased from rapid evaporations (∼0.1 mL/h), the microstructure evolved from a totally disordered one sequentially to inverted phases consisting of spheres and then cylinders of polybutadiene (PB) in a PS matrix and finally reached the equilibrium phase, namely cylinders of PS in a PB matrix. We interpret the formation of inverted phases as due to the increased relative importance of entropy as $\chi_{eff}Z$ is decreased, which may dominate the energy penalty for having a bigger interfacial area between the immiscible blocks in the inverted phases.

Introduction

Polymers are ideal for making nanostructure materials since the typical radius of gyration of a polymer chain is on the order of nanometers.[1] Block copolymers are especially interesting for these applications because of their ability to self-assemble into a varieties of ordered phases.[2] These structures arise as the system strives to satisfy the delicate balance between minimizing the unfavorable interaction energy between the incompatible blocks and maximizing the conformational entropy of the system. Therefore, the appearance of a particular microstructure depends strongly on the volume fractions, chemistry, and architecture of the constituent blocks. Block copolymers belong to a special class of materials—soft condensed matter. In contrast to crystalline solids, they form ordered states having fluidlike disorders on the molecular scale wherein the dominating thermodynamic factor is entropy, and yet a high degree of order exists in larger length scales.[3] This complexity in their ordered structures can give block copolymers many interesting and sometimes intriguing properties.

In the strong segregation regime of a diblock copolymer melt (χN >100, where *N* is the total degree of polymerization of the block copolymer and χ the Flory−Higgins interaction parameter), the morphology of the equilibrium microstructure is dependent only on the volume fraction of the minority block, *f* (or alternatively, that of the majority block, $(1 - f)$). But when the system is under conditions near the ODT, i.e., in the weak segregation limit, the phase behavior of the block copolymer will become also dependent on the combination parameter, χN. Using the Landau mean-field theory, Leibler[4] calculated the phase diagram for microphase separations of a diblock copolymer in the weak segregation limit and is shown in Figure 1. In particular, for $f = {}^1/_2$, the ODT occurs if $\chi N = 10.495$. According to the phase diagram (Figure 1), as χN is lowered, the equilibrium morphology changes from lamellae to the disordered state via cylinders and spheres, except for the symmetric diblock $f = 0.5$. Since χ is related to the reciprocal of the absolute temperature, *T*, the series of morphological transitions (order−order transitions) can in principle be induced via temperature changes and has been observed by various researchers.[5−14]

For diblock copolymers in nonselective good solvents, recent mean-field theories[15,16] suggested that the phase behavior in the semidilute regime (where the ODT occurs[16]) was determined by a different combination parameter, namely $\chi_{eff}Z$, where $\chi_{eff} = \alpha\chi/(1 + \chi_S)^2\varphi^{\chi_S/(3\nu-1)}$ and *Z* the number of "blobs" of size equal to the correlation length[1] contained in a block copolymer = $N\varphi^{1/(3\nu-1)}$. (Here, φ is the volume fraction of the polymer in the solution, and α is a constant of the order 1; $\chi_S = 0.22$, $\nu = 0.588$ for good solvents.) Therefore, the new combination parameter $\chi_{eff}Z$ can also be written as $\chi' N\varphi^{1.6}$ for good solvents, where $\chi' = \alpha\chi/(1 + \chi_S)^2$. According to Fredrickson and Leibler,[15] the phase diagram for a long block copolymer chain in nonselective good solvents is shown in Figure 2. Clearly, $\chi_{eff}Z$ replaces the role played by χN in the phase diagram for

[†] Chinese Academy of Sciences.
[‡] Hong Kong University of Science and Technology.
* To whom correspondence should be addressed. E-mail tbhe@ns.ciac.jl.cn (T.H.) and phtsui@ust.hk (O.K.C.T.)

10.1021/ma001161q CCC: $19.00
Published on Web 11/30/2000

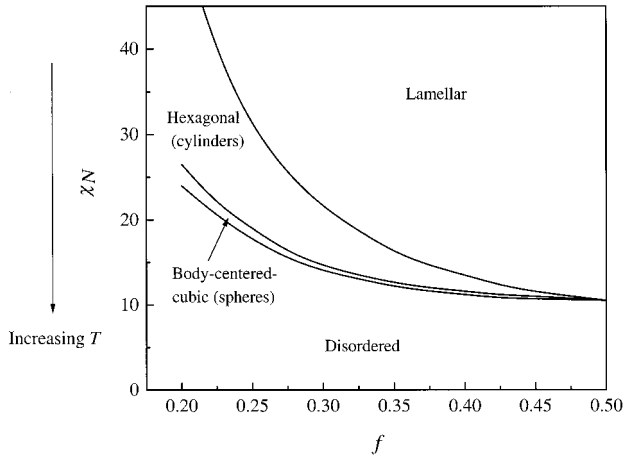

Figure 1. Phase diagram according to Leibler (based on Figure 8 of ref 4). The ODT can be driven by changes in temperature as indicated.

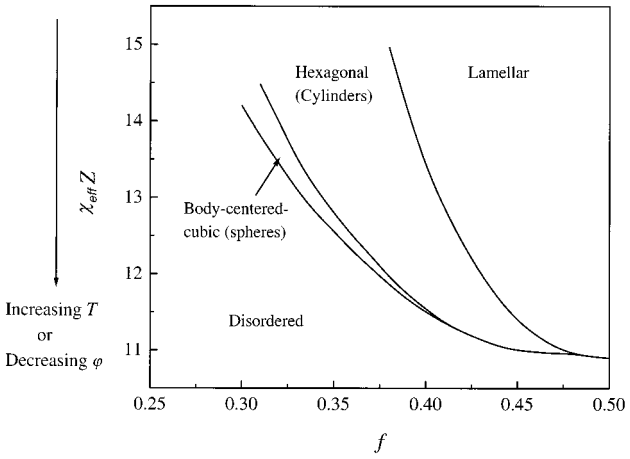

Figure 2. Phase diagram of Fredrickson and Leibler (based on Figure 3 of ref 15) for block copolymers with $Z = 10^6$ in nonselective good solvents in the semidiluate regime. The ODT can be induced by changes in temperature or solution concentration as indicated.

block copolymer melts. Therefore, phase transitions can also be driven by changes in the polymer solution concentration, φ besides via changes in T. Experimental investigations of solvent-induced ODT using mainly small-angle X-ray scattering (SAXS)[17−20] and complex rheology and optical measurements[21,22] had been reported. In these studies, either φ, T, or N was controlled, wherein an increase in φ always leads to a decrease in the transition temperature and $\varphi \sim N^{-1/2}$ at ODT,[18] in reasonable agreement with the mean-field theory of Fredrickson and Leibler.[15] However, systematic investigation of the structural transitions as $\chi_{\text{eff}}Z$ varies is still not available. This is mainly due to kinetic reasons:[17−21] The system is locked up to nonequilibrium structures, especially at large φ or small T, because the free energy barrier leading to the equilibrium structure is too large to surmount. On the other hand, at small φ, direct inspection of the microstructure is difficult by SAXS due to the small signal intensity.[17] In the present study, we *make use of the kinetics* to freeze in the microstructure of solution-cast SBS films at successive values of $\chi_{\text{eff}}Z$. It was realized by using different evaporation rates for making different films. Kinetic arrest of the chains in the film occurs when concentration of the film increases (because of evaporation) to the point where the copolymer undergoes glass transition at the experimental conditions, which is ambient in this experiment. Clearly, the faster the evaporation rate, microstructures of smaller $\chi_{\text{eff}}Z$ will be frozen in as the polymer chains are given less time to rearrange to the equilibrium microstructures for the later stages of the evaporation process. This approach should be especially suitable for realization of microstructures corresponding to smaller φ (hence smaller $\chi_{\text{eff}}Z$) where the chains are more mobile to rearrange into the structure.

To study the morphologies, we used both bright-field TEM (BF-TEM) and tapping mode atomic force microscopy (TM-AFM). The former has been used extensively in the past for morphological studies of polymers. It provides direct visualization of the microstructure and yields local details. However, the technique requires sectioning of the study object, and sometimes sample staining is required. More recently, AFM has become widely accepted as an alternative tool to the traditional ones,[23] owing to the ease of sample preparation and its ability to yield nanometer-scale structural information. In this study, TM-AFM was chosen by virtue of the convenient sample preparation. BF-TEM was chosen due to its ability to unambiguously identify different domains in the microstructures with the aid of selective sample staining.

Our results revealed a series of transitions in the microstructure in going from spheres to cylinders as the evaporation rate was decreased (hence χ_{eff} increased), analogous to the order−order transition observed by others[5−13] by thermal means. What is the most intriguing is that those microstructures obtained at sufficiently fast evaporation rates are inverted (i.e., the microdomains—the spheres and/or the cylinders—are composed of the *majority* block). Existence of inverted phases has been predicted[24] and experimentally observed[21] by Williams and co-workers. In this paper, we report more systematic observations, by direct imaging means, of successive unfolding of different inverted phases as χ_{eff} varied. The occurrence of inverted phases can be physically understood as due to dominance of the short-range entropic effects over the long-range orders, which is a unique characteristic of orderings in soft condensed matter.[3]

Experimental Section

The sample poly(styrene-*b*-butadiene-*b*-styrene) (SBS) triblock copolymer was purchased from Aldrich Chemical Co. (Milwaukee, WI). It has a weight-averaged molecular weight of 140K Da, polydispersity index 1.2 (LC-4A liquid chromatographer, Shimadzu Corporation, Kyoto, Japan), and PS weight fraction 30%. According to quantitative ^{13}C NMR spectral analyses (Unity 400 NMR, Varisan, Palo Alto, CA), the butadiene block contains 60.5% *trans*-1,4, 29.5% *cis*-1,4, and 10% vinyl isomeric units. The triblock copolymer was dissolved in either carbon tetrachloride or toluene to produce 0.5 wt % solutions. The resultant solution was cast onto surfaces of freshly cleaved mica. Tables 1 and 2 list the vapor pressures of the two solvents near room temperature,[25] showing clearly that carbon tetrachloride is much more volatile. The more volatile SBS in carbon tetrachloride was used to produce sample A. The cast film was allowed to dry under ambient condition (~25 °C) until no further weight loss was observed. We found that >95% of the drying out was completed in a few minutes. The less volatile SBS in toluene was used to prepare the other samples for which the solvent evaporation rate, R was varied. To control R, a cast film (on mica) was put inside a glass vessel with a $^1/_4$ in. diameter constricted opening to which a rubber hose was connected (Figure 3). The evaporation rate inside the vessel is controllable by adjusting the tension applied to a clamp that mechanically squeezes the rubber hose

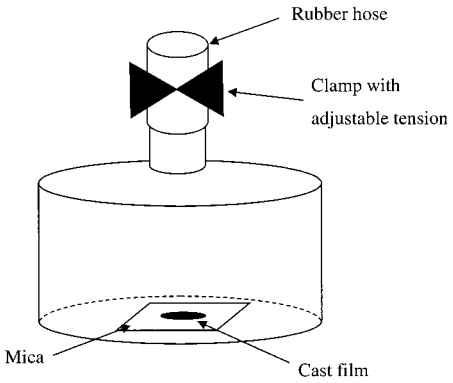

Figure 3. Schematic illustration for the setup used in this experiment to control the solvent evaporation rate.

Table 1. Vapor Pressures of Carbon Tetrachloride near the Room Temperature

temperature (°C)	vapor pressure (mmHg)
12.3	60
23	100
38.3	200

Table 2. Vapor Pressures of Toluene near the Room Temperature

temperature (°C)	vapor pressure (mmHg)
18.4	20
31.8	40
40.3	60

(Figure 3). In the order of decreasing evaporating rates, samples B−E were prepared with estimated evaporation rates ca. 0.1, 0.01, 0.001, and 0.00005 mL/h, respectively.

Tapping mode AFM was carried out in a commercial scanning probe microscope (NanoScope IIIa, Digital Instruments Inc., Santa Barbara, CA) equipped with an integrated silicon tip/cantilever with resonance frequency ∼100 kHz from the same manufacturer. Since the difference in mechanical properties between the glassy PS block and the rubbery PB block was substantial, phase imaging in TM-AFM was used to differentiate the two components. During operations, the driving amplitude, A_0, of the AFM was ∼20 nm, and the set-point amplitude ratio, $\gamma_{sp} = A_{sp}/A_0$ (where A_{sp} was the set-point amplitude), was maintained at 0.6−0.7, corresponding to moderate tapping.[26]

BF-TEM was conducted in a JEOL 2010 TEM with an accelerating voltage of 200 kV. As BF-TEM serves to confirm the identity of individual components (i.e., PS or PB) in the TM-AFM images, only a subset of samples was studied. Specimens to be examined were stained with OsO_4 for 20−30 min. Since OsO_4 selectively reacts with the double bonds in PB, the stained PB domains will scatter electrons more strongly. Therefore, dark regions in a BF-TEM image can be identified with the PB domains.

Results and Discussion

The miscibility between a polymer and a solvent is governed by the polymer−solvent interaction parameter, $\chi_{ps} = V_1(\delta_1 - \delta_2)^2/RT + 0.34$,[27] where the first term is the enthalpic component and the second one the entropic component; V_1 is the molar volume of the solvent, R the gas constant, and δ_i the solubility parameters (i = polymer or solvent). According to the literature, solubility parameters of PS, PB, carbon tetrachloride, and toluene are respectively 16−17.6, 17−19.8, 17.6, and 18.2 $MPa^{1/2}$;[27] V_1 of carbon tetrachloride and toluene are 96.5 and 102.95 cm^3, respectively.[28] One may then find that χ_{ps} for PS and PB in carbon tetrachloride (or toluene) are essentially the same, ∼0.365 (0.367) ± 0.005. Furthermore, using the Flory−Higgins criterion for complete solvent−polymer miscibility i.e., $\chi_{ps} < 0.5$, both solvents should be nonselective good solvents for the SBS block copolymer. Therefore, the theory by Fredrickson and Leibler[15] should be usable as a guideline for this sample.

The PS−PB interaction parameter, α (mol/m^3), has been determined previously by Rounds:[19]

$$\alpha = -900 + 7.5 \times 10^5/T \quad (1)$$

It is related to χN by the simple relation[30]

$$\chi N = \alpha(M_{W,PS}\nu_{PS} + M_{W,PB}\nu_{PB}) \quad (2)$$

where $M_{W,PS}$ ($M_{W,PB}$) is the weight-average molecular weight of PS (PB) and ν_{PS} (ν_{PB}) the specific volume of PS (PB) = 0.9199 (1.1138) cm^3. For the SBS sample used in the present study, $M_{W,\,PS}$ = 42K Da and $M_{W,\,PB}$ = 98K Da. Therefore, we have

$$\chi N = -133 + 1.1 \times 10^5/T \quad (3)$$

for our SBS sample. At T = 25 °C (298 K), it gives χN = 236, which puts the sample in the strong segregation limit. According to the phase diagram shown in Figure 1, one expects the ODT to occur at $\chi N \approx 15$ for f = 24.5% (obtained by assuming a PS weight fraction of 30% and values of ν_{PS} and ν_{PB} given above), if we ignore any difference in phase behaviors between diblocks and triblocks which should be justifiable when $f \lesssim 20\%$.[30] If the ODT is driven by increasing T, the transition should take place at 743 K, i.e., 470 °C. However, it is not realizable since the SBS sample will have been thermally degraded well before the transition is reached. On the other hand, it is realizable by solvent-induced ODT. Using Fredrickson and Leibler's mean-field calculations shown in Figure 2, we estimate that the transition will occur at φ = 26.5%, consistent with typical values found experimentally.[17−20] However, we note that the phase diagram in Figure 2 had been calculated for a much longer chain with $Z = 10^6$. If the present estimate correctly reflects the reality, the chains should still be quite mobile to rearrange into forming the equilibrium morphology.[20] Hence, one should be able to study the ODT by solvent induction for this sample via the scheme outlined above in the Experimental Section.

The TMAFM phase image of sample A is shown in Figure 4a. As seen, no sign of ordering is evident in this sample. At a starting polymer concentration of 0.5 wt %, the copolymers in the as-cast film were disordered according to the above estimate. Under the fast evaporation rate imposed on sample A, the film concentrated rapidly. Kinetic arrest in the polymer might have taken place before the chains had enough time to make the rearrangements needed to attain *any* equilibrium morphology occurred in the course of the evaporation. This is analogous to fast quenching of a disordered block copolymer melt from elevated temperatures.

TM-AFM phase images of samples B−D are shown respectively in Figure 4b−d, which clearly show that there are ordered structures in these samples. Apparent in the images, the brighter domains take up more than 50% of the total area. Since 70 wt % of our SBS sample is PB, it is natural to expect the brighter domains to contain the PB blocks. With a small driving amplitude of the tip ($A_0 \sim 20$ nm) and moderate tapping (γ_{sp} = 0.6−

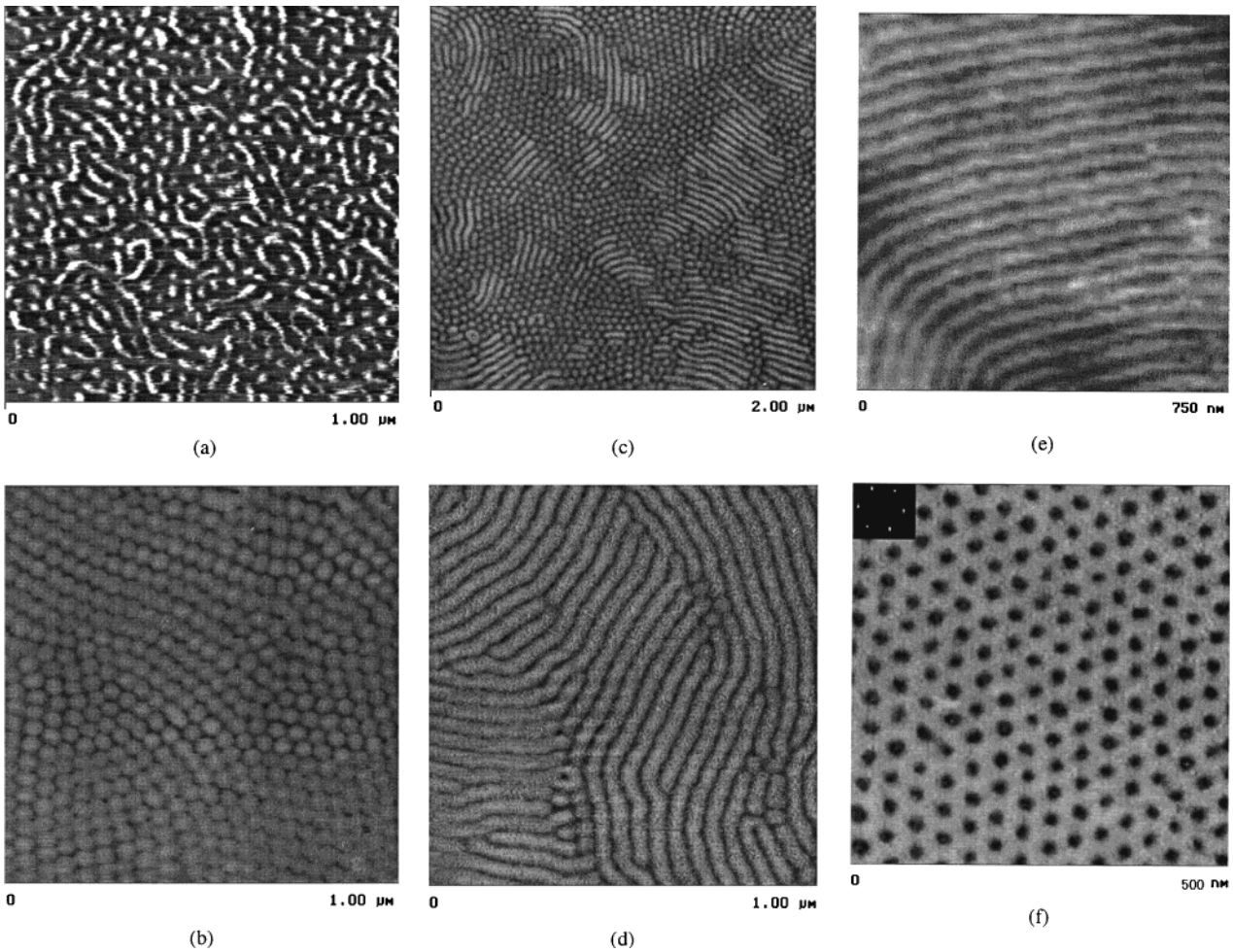

Figure 4. Tapping mode AFM phase images obtained from (a) sample A, (b) sample B, (c) sample C, (d) sample D, (e) a thick region in sample E, and (f) a thin region in sample E.

0.7), the phase shift in the *ac* tip response is dominated by weak, attractive tip−sample interactions. Bar et al.[26] showed that the more compliant component would appear brighter in the TM-AFM phase images under these conditions. This is in keeping with our speculation for the domain components in Figure 4b−d and recent TM-AFM studies of Raghavan et al.[31] on PS/PB blend films. To unambiguously identify the PS and PB domains in the microstructures, the same samples were stained with OsO_4 and reexamined by TEM. Figure 5a−c displays the BF-TEM images obtained for samples B−D, respectively, which evidently show that our original assignment for the microdomain components in the TM-AFM phase images was correct. One may thus conclude that the microstructures shown in parts a and b of Figure 5 (i.e., samples B and C) are spheres and/or cylinders of PB in a matrix of PS. It has yet to determine the morphologies of these samples. For sample B, since both the AFM micrograph in Figure 4b (which reveals the surface morphology) and the TEM micrograph in Figure 5a (which reveals the morphology in the cross section of the film) are showing only spheres, the morphology should be spherical. As for sample C, the circular features found in Figures 4c and 5b can very well be cross sections of cylinders. Therefore, the morphology can either be pure cylinders or a mixture of spheres and cylinders. On the basis that surface effects will force the cylinders to lie parallel to the free surface,[32,33] the circular features observed in the AFM micrograph (in Figure 4c) is unlikely to be perpendicular cylinders. Hence, we deduce that they are most probably spheres, and the morphology of sample C is a coexistence of spheres and cylinders. It is agreeable that a more reliable check for the distinction is by SAXS.[14] However, the SAXS intensity of the higher order peaks of sample C was too weak to be discernible, probably due to the interface between the PS and PB being too broad,[20] which is expected if the microstructure has been formed where χ_{eff} (or φ) was small. Nonetheless, it is clearly evident that the morphology changes from spherical to one that contains cylinders in going from sample B to sample C. The identification for Figure 5c (i.e., sample D) is more difficult. On the basis of the disclination defect distinguished by the white arrow in the figure and similar ones that are also found in the TM-AFM phase image of the same sample (Figure 4d), we conclude that the matrix phase is also PS in this sample. Keller and co-workers[34] pointed out that SBS block copolymer melts with ∼30 wt % PS should have microstructures consisting of PS cylinders in a matrix of PB. In a system that microphase separates, the total free energy is determined by the interaction energies between the incompatible components and contributions from the configurational entropy. In a polymer system, the former usually dominates,[2] so one expects the spherical and/or cylindrical microdomains to be composed of the minority component so as to minimize the interfacial interaction energies between the immiscible domains. We refer to this phase structure—one that consists of spheres and/or cylinders

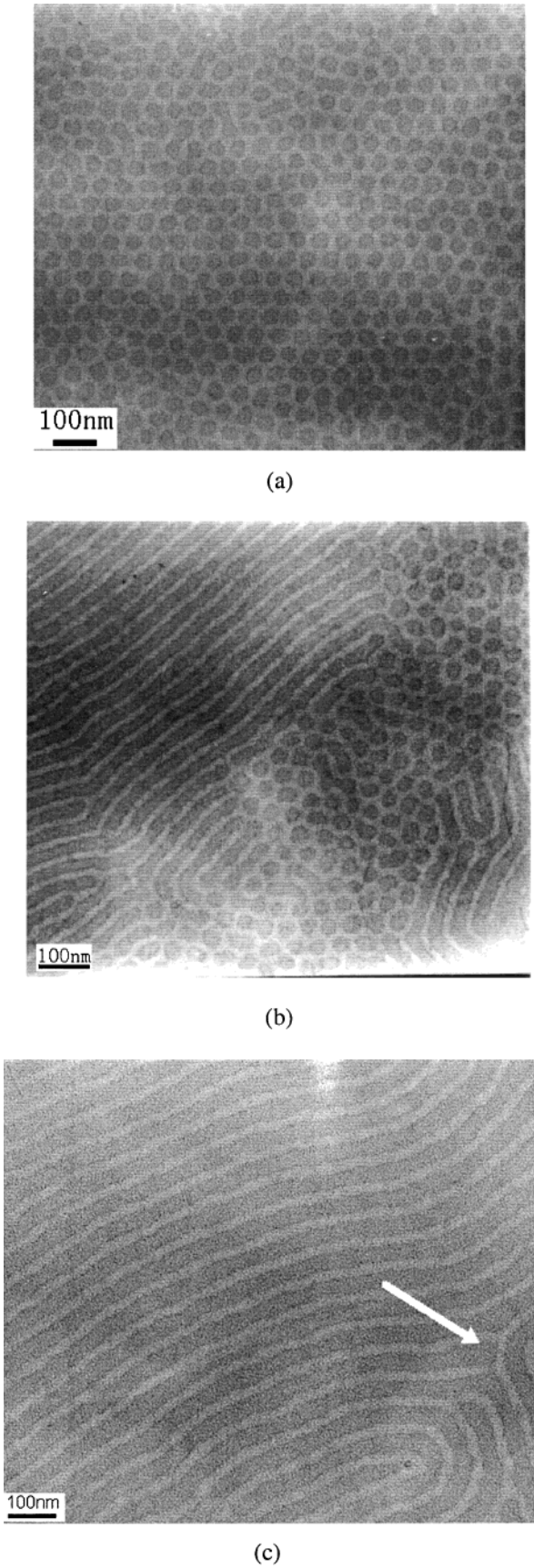

Figure 5. (a−c) Bright-field TEM micrographs of samples B−D. Samples had been OsO_4 stained to enhance the contrast. Therefore, the dark regions are the PB domains. The white arrow in (c) points at a disclination defect.

of the minority block in a matrix of the majority block—the "normal phase". With respect to the normal phase, phase structures identified for samples B−D in Figures 4b−d and 5a−c, being consisted of spheres and/or cylinders of the majority block in a matrix of the minority block, are therefore inverted. Their formation is counter to the thermodynamic reasoning given above for the normal phase. We refer to this phase structure the "inverted phase" and the associated phenomenon the "phase inversion".

We further notice that there are interesting order−order transitions noticeable from the different microstructures found in different samples. Recall that microstructures of samples B−D correspond to ones with increasing effective interaction parameter, χ_{eff}. Our results suggest that as χ_{eff} was increased, the microstructure evolves from spherical (sample B) to cylindrical (sample D) through a transitional state of coexisting spheres and cylinders (sample C). Similar order−order transitions had been observed in block copolymer melts by thermally induced ODT.[5−14] The systematic order−order transition observed in the present study occurs in solution-cast polymer films by solvent-induced ODT. If we assume that the spheres are arranged in a bbc structure, which is predicted by the theories[4,15] and confirmed by the experiments,[6,14] the spherical microdomains displayed in Figure 4b,c or 5a,b for samples B and C, respectively, belong to the (111) plane. Hashimoto and co-workers[14] proposed that the transition from spheres to cylinders took place by coalescence of spheres along either the [111] or the three principal axes in the (111) plane, namely the $[\bar{1}\bar{1}2]$, $[\bar{1}2\bar{1}]$, and $[2\bar{1}\bar{1}]$ directions, through a transitional state of undulated cylinders. This picture of the elemental process is consistent with the microstructures we found for sample C (Figures 4c and 5b), in which the cylinders seem to grow along the three principal directions emanating from the spherical microdomains.

When the solvent evaporation rate is extremely slow, one expects the ultimate equilibrium state—the cylindrical normal phase—to form.[4,15,34] Shown in Figure 4e,f are the TM-AFM phase images of sample E, for which an extremely slow evaporation rate of ~0.000 05 mL/h was imposed. Figure 4e was obtained near the edge of the film where the film was visibly thicker, whereas Figure 4f was obtained in the center of the film where the film was visibly thinner. The inset of Figure 4f shows the Fourier transformation of the image in the main panel of the same figure. These results unambiguously confirm that the microstructure of sample E is a hexagonal array of PS cylinders in a matrix of PB, conforming to the equilibrium microstructure expected. The different facets of the morphology revealed by Figure 4e,f can be understood as a result of the interplay between surface effects and confinement effects. At the interfaces of a block copolymer film, the block with the lowest specific interaction energy with the interfacial wall will preferentially wet the surface of the wall. In PS−PB block copolymer films, for example, the lower surface tension PB was found to segregate to the free surface.[32] Such surface effects will force the microdomains to lie parallel to the surface in its proximity.[33] In thin block copolymer films where the film thickness, t, is several times the natural period, L_0, of the microdomain structure, the surface effects may be able to extend over the entire thickness of the film, giving rise to a global parallel orientation of the microstructure. This accounts for the parallel morphology found in Figure 4e. However, there are also frustration effects

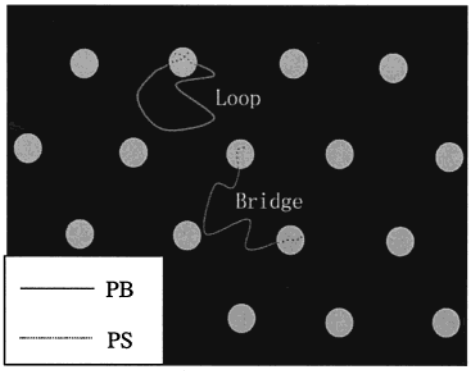

Normal Phase (PS cylinders in a PB matrix)

(a)

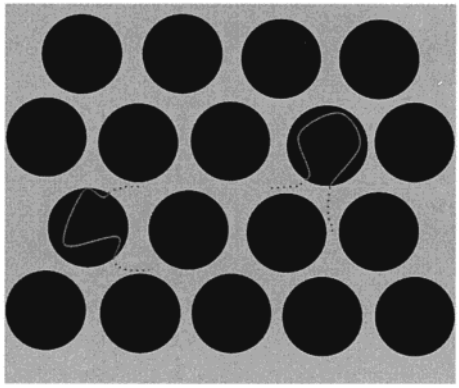

Inverted Phase (PB cylinders or spheres in a PS matrix)

(b)

Figure 6. Schematic illustration for the SBS microstructure and the corresponding allowed polymer chain configurations in (a) the normal phase and (b) the inverted phase. In this illustration, the light gray regions correspond to the PS domains, and the dark regions correspond to the PB domains.

coming from incommensurability between t and L_0,[35,36] which have been found to cause perturbations to the period of the microstructure.[37,38] As the film thickness is reduced, mean-field calculations show that frustration effects will exacerbate.[35,36] Kellogg et al.[39] found that when frustration effects overcame the surface effects, perpendicular ordering of the block copolymer could be observed. We believe that the perpendicular morphology found in Figure 4f is due to divergence in frustration effects in very thin regions of the film, which had dominated the surface effects.

We shall now elaborate the physical picture for the formation of inverted phases. Consider the schematic illustrations shown in parts a and b of Figure 6 for the normal and the inverted phase, respectively. As seen, the amount of restriction on the allowed chain configurations can be quite different in the two phases. In the normal phase (Figure 6a), the two styrene end blocks are either distributed in different PS domains resulting in a "bridge" or coexist in the same PS domain resulting in a "loop".[40] In both cases, the relative orientation between the two ends of the middle block is limited; i.e., they are constrained to the small solid angle subtended by one small PS domain at the other. In the inverted phase (Figure 6b), on the other hand, the styrene blocks constitute the matrix. Therefore, the styrene end blocks can have a much bigger degree of freedom to fill the space. Therefore, the inverted phase is foreseeable to be entropically more favorable. The other issue to consider is enthalpy. In dilute solutions of segregated block copolymers where $\chi_{eff}Z$ is small, Fredrickson and Leibler's calculations[15] showed that there would be enrichment of solvent molecules at the interface between the two phases, giving rise to substantial screening of the unfavorable interactions between the two immiscible blocks. Both factors work to lessen the relative importance of the enthalpic factors with respect to the entropic ones in microphase separation of block copolymer solutions. In sufficiently dilute solutions, it is possible that the entropic factors overwhelm the enthalpic ones, leading to favoritism of the inverted phases.[24] We note, however, that the above discussions are applicable only to ABA triblocks with A being the minority block. Indeed, as far as we are aware of, observations of inverted phases had not been reported on solvent-induced ODT studies of AB diblocks. However, it does not exclude the possibility that the inverted phases found here are simply metastable states being frozen in by the fast evaporation processes. In the immediate future, we plan to repeat the studies on a SB diblock copolymer. Nevertheless, our results unambiguously demonstrate that controlled solvent evaporation of block copolymer solutions offers a new route for making new self-assembled block copolymer microstructures.

Conclusion

By controlling the evaporation rate of solution-cast SBS block copolymer films, we were able to freeze in different microstructures corresponding to different effective interaction parameter, χ_{eff}, of the drying films (where microstructures of the lower χ_{eff} were frozen in at higher evaporation rates.) At evaporation rates $\gtrsim$0.001 mL/h (but $\lesssim$0.1 mL/h), inverted phases consisting of spheres and/or cylinders of the majority block were found, which were not predicted on the basis of typical thermodynamic considerations for block copolymer melts. At a slower evaporation rate, however, the normal phase recovered. The series of inverted phases observed also evidenced an interesting solvent-induced order−order transition, where spheres were transformed into cylinders as the effective interaction parameter was increased upon decreasing the solvent evaporation rate. The formation of inverted phases was explained in terms of the relative importance of entropy in dilute triblock copolymer solutions, which may overcompensate for the enthalpic penalty for having a larger total interfacial area in the inverted phases.

Acknowledgment. We thank Dr. D. A. Hajduk for useful discussions. This work was supported by National Science Foundation of China under Grant 29425005. O.K.C.T. acknowledges support by the Polymer Physics Laboratory, Changchun Institute of Applied Chemistry, under Project R120001W and the Williams Mong Solid State Clusters Laboratory, Hong Kong University of Science and Technology.

References and Notes

(1) de Gennes, P. G. *Scaling Concepts in Polymer Physics*; Cornell University Press: Ithaca, NY, 1979.
(2) Bates, F. S.; Fredrickson, G. H. *Annu. Rev. Mater. Sci.* **1990**, *41*, 425.

(3) Bates, F. S.; Fredrickson, G. H. *Phys. Today* **1999**, *52*, 32.
(4) Leibler, L. *Macromolecules* **1980**, *13*, 1602.
(5) Almdal, K.; Kopi, K. A.; Bates, F. S.; Mortensen, K. *Macromolecules* **1992**, *25*, 1743.
(6) Sakurai, S.; Kawada, H.; Hashimoto, T.; Fetters, L. J. *Macromolecules* **1993**, *26*, 5796.
(7) Hajduk, D. A.; Harper, P. E.; Gruner, S. M.; Honeker, C. C.; Kim, G.; Thomas, E. L.; Fetters, L. J. *Macromolecules* **1994**, *27*, 4063.
(8) Hajduk, D. A.; Gruner, S. M.; Rangarajan, P.; Register, R. A.; Fetters, L. J.; Honeker, C.; Albalak, R. J.; Thomas, E. L. *Macromolecules* **1994**, *27*, 490.
(9) Förster, S.; Khandpur, A. K.; Zhao, J.; Bates, F. S.; Hamley, I. W.; Ryan, A. J.; Bras, W. *Macromolecules* **1994**, *27*, 6922.
(10) Koppi, K.; Tirrell, M.; Bates, F. S.; Almdal, K.; Mortensen, K. *J. Rheol.* **1994**, *38*, 999.
(11) Khandpur, A. K.; Förster, S.; Bates, F. S.; Hamley, I. W.; Ryan, A. J.; Bras, W.; Almdal, K.; Mortensen, K. *Macromolecules* **1995**, *28*, 8796.
(12) Sakurai, S.; Hashimoto, T.; Fetters, L. J. *Macromolecules* **1996**, *29*, 740.
(13) Vigild, M. E.; Almdal, K.; Mortensen, K.; Hamley, I. W.; Fairclough, J. P. A.; Ryan, A. J. *Macromolecules* **1998**, *31*, 570.
(14) Kimishima, K.; Koga, T.; Hashimoto, T. *Macromolecules* **2000**, *33*, 968.
(15) Fredrickson, G. H.; Leibler, L. *Macromolecules* **1989**, *22*, 1238.
(16) Olvera de la Cruz, M. J. *Chem. Phys.* **1989**, *90*, 1995.
(17) Shibayama, M.; Hashimoto, T.; Kawai, H. *Macromolecules* **1983**, *16*, 16.
(18) Hashimoto, T.; Shibayama, M.; Kawai, H. *Macromolecules* **1983**, *16*, 1093.
(19) Shibayama, M.; Hashimoto, T.; Hasegawa, H.; Kawai, H. *Macromolecules* **1983**, *16*, 1427.
(20) Shibayama, M.; Hashimoto, T.; Kawai, H. *Macromolecules* **1983**, *16*, 1434.
(21) Pico, E. R.; Williams, M. C. *Polym. Eng. Sci.* **1977**, *17*, 573.
(22) Hugenberger, G. S.; Williams, M. C. *Macromolecules* **1988**, *21*, 1773.
(23) (a) Binnig, G.; Quate, C. F.; Gerber, Ch. *Phys. Rev. Lett.* **1986**, *56*, 930. (b) Magonov, S. N.; Reneker, D. H. *Annu. Rev. Mater. Sci.* **1997**, *22*, 175.
(24) Pico, E. R.; Williams, M. C. *J. Polym. Sci., Polym. Phys.* **1977**, *15*, 1585.
(25) Stall, D. R. *Ind. Eng. Chem.* **1947**, *39*, 517.
(26) Bar, G.; Thomann, Y.; Brandsch, R.; Cantow, H.-J. *Langmuir* **1997**, *13*, 3807.
(27) *Polymer Handbook*, 2nd ed.; Brandrup, J., Immergut, E. H., Eds.; John Wiley & Sons: New York, 1975.
(28) *Catalog Handbook of Fine Chemicals*; Aldrich Chemical Co.: Milwaukee, WI, 1998.
(29) Rounds, N. A. Ph.D. Dissertation, University of Akron, Akron, OH, 1970.
(30) Han, C. D.; Kim, J.; Kim, J. K. *Macromolecules* **1989**, *22*, 383.
(31) Raghavan, D.; Gu, X.; Nguyen, T.; Vanlandingham, M.; Karim, A. *Macromolecules* **2000**, *33*, 2573.
(32) Harrison, C.; Park, M.; Chaikin, P.; Register, R. A.; Adamson, D. H.; Yao, N. *Macromolecules* **1998**, *31*, 2185.
(33) Henkee, C. S.; Thomas, E. L.; Fetters, L. J. *J. Mater. Sci.* **1988**, *23*, 1685.
(34) Keller, A.; Pedemonte, E.; Willmouth, F. M. *Polymer* **1970**, *238*, 385.
(35) Turner, M. S. *Phys. Rev. Lett.* **1992**, *69*, 1788.
(36) Walton, D. G.; Kellogg, G. J.; Mayes, A. M.; Lambooy, P.; Russell, T. P. *Macromolecules* **1994**, *27*, 6225.
(37) Lambooy, P.; Russell, T. P.; Kellogg, G. L.; Mayes, A. M.; Gallaugher, P. D.; Satija, S. K. *Phys. Rev. Lett.* **1994**, *72*, 2899.
(38) Mansky, P.; Russell, T. P. *Macromolecules* **1995**, *28*, 8092.
(39) Kellogg, G. J.; Walton, D. G.; Mayes, A. M.; Lambooy, P.; Russell, T. P.; Gallagher, P. D.; Satija, S. K. *Phys. Rev. Lett.* **1996**, *76*, 2504.
(40) Matsen, M. W. *J. Chem. Phys.* **1995**, *102*, 3884.

MA001161Q